

## Terrain influences on the dynamics of heat lows

By Zsuzsanna Reichmann\* and Roger K. Smith

*Meteorological Institute, University of Munich*

August 20, 2002

### Abstract

The hydrostatic primitive-equation numerical model we used earlier to study the basic dynamics of heat lows in an idealized flow configuration is extended to investigate the effects of orography. Calculations are carried out over a heated land mass with an elevated plateau for the case with no surrounding sea, as well as with the sea present. We investigate the effect of the shape of the terrain on the mature heat low. In the presence of orography the mixed layer over land becomes deeper than without orography and the induced flow is stronger also. The width of the plateau influences among other things the relative vorticity distribution and the nocturnal jet development. The flow behaviour in the presence of orography provides an explanation for the different vertical profiles of vertical velocity in heat lows discussed in the literature.

### 1. INTRODUCTION

Over significant land masses, especially at low latitudes during the warmer and drier months, a large surface sensible heat flux to the atmosphere results in a relatively deep convectively well-mixed boundary layer during the day. Such regions are normally associated with low surface pressure and a cyclonic circulation below about 700 hPa. These so-called heat troughs or heat lows may be thought of as low-level maxima in cyclonic relative vorticity which are linked to horizontal gradients of diabatic heating. Heat lows are important for several reasons: they interact with low latitude fronts and with upper level troughs; they influence the pattern of low-level flow, which, in turn, may determine preferred regions in which deep convection might be triggered and/or where polluted air might be transported; and they may play a role in monsoon development. It may be significant that heat lows occur mostly over regions of elevated terrain (Australia, Iberian Peninsula, Mexico, Tibetan Plateau). Indeed, several papers have alluded to the importance of orography, but its dynamical influence remains to be elucidated.

The low-level airflow over northern Australia is dominated by two surface heat troughs in the easterlies for much of the year. The stronger of the two is normally the one centred over northwestern Australia, typically over the elevated terrain of the Pilbara and Kimberley Ranges, while the second trough develops over the Cloncurry area in Queensland. Model solutions by Fandry and Leslie (1984) indicate that orography is of only marginal importance in producing the western trough, whereas the high east coast orography is significant in the formation of the eastern trough. Hart (1990) investigated mean vertical velocity profiles over northern Australia for January, a time of year when heat lows are prominent synoptic features in this region. He inferred a deep layer of ascending motion in the evening in contrast to other studies, such as that over Saudi Arabia by Blake *et al.* (1983), where ascent occurred only below 800 hPa and only during the day. The significant downward motion found by Hart occurs in the morning hours only at heights above the 600 hPa level under cloudless skies. We show below that this difference can be attributed to the orography. Hart examined the suggestion by Otterman (1974) and Charney (1975) in the

\* Corresponding author address: Ms. Zsuzsanna Reichmann, Meteorological Institute, University of Munich, Theresienstr. 37, 80333 Munich, Germany, Email: zsuzsa@meteo.physik.uni-muenchen.de

context of the Sahel drought, that increases of surface albedo in semi-arid regions associated with human activity modify the surface radiation budget so as to enhance subsidence over the region. He argued that this could only be a minor effect over northern Australia. The most striking feature of the vertical velocity profiles is their strong diurnal variation, particularly in the vertical velocity. Hart observed that the diurnal variation is not just confined to the coast, the changes in vertical motion occur also inland over the plateau. Using a linearized analytic model, Adams (1993) compared the flows induced by orographic forcing and heat-induced forcing when the orographic distribution and the heating distribution have a similar structure. He showed that the two responses have many similarities. Both forcing mechanisms excite downstream waves with the same wavelength.

Over Europe, the heat low that forms over the Iberian Peninsula is a prominent feature of the low-level flow in summer. Gaertner *et al.* (1993) showed that the strength of the low is closely related to terrain characteristics. They noted that three forcing mechanisms dominate the dynamics over the northern part of the Peninsula during the summer: the land-ocean thermal contrast; the existence of topographic features and the land cover inhomogeneities. Their results suggest that the difference in the depth of the well-mixed layer between the lower lying areas to the south of the plateau and the plateau, itself, is the main factor determining the thermal low intensity.

In a recent paper, we described a numerical study of the basic dynamics of heat lows over a level heated land mass surrounded by sea (RÁCZ and Smith 1999, hereafter referred to as RS). The study helps to understand some of the observed aspects of heat lows, including their shallow nature, the existence of a convergent cyclonic circulation at low levels, a divergent anticyclonic circulation aloft, the late afternoon timing of the minimum surface pressure, and the maximum relative vorticity at night. The same numerical model is used here to investigate the effects of orography on the dynamics of heat lows in idealized flow configurations with a quiescent environment. Calculations are carried out for the case of plateau with no surrounding sea, as well as with the sea present.

A brief description of the numerical model is given in Section 2, and the results of the numerical experiments are presented in Section 3. A summary of the results and the conclusions are presented in Section 4.

## 2. THE NUMERICAL MODEL

The model used is the hydrostatic, primitive-equation, numerical model formulated in  $\sigma$ -coordinates  $(x, y, \sigma)$  on a Southern Hemisphere f-plane described by RS, to which a simple radiation scheme has been added. The horizontal coordinates  $(x, y)$  refer to the zonal and meridional directions and  $\sigma = p/p_s$ , where  $p$  and  $p_s$  are the pressure and surface pressure, respectively. The radiation scheme is that used by Raymond (1994) and includes a solar radiation heating profile, a long-wave cooling rate and diurnal variation in the troposphere. The details of the scheme are given in the Appendix. We summarize the salient features of the model in Table 1. The model equations and method of solution are detailed by RS.

### (a) *Initial conditions and experimental design*

Calculations are carried out to investigate the effects of the orography on the dynamics of heat lows. The range of numerical experiments is summarized in Table 2. In the first two experiments there is elevated terrain in the centre of the computational domain. The height of the terrain in metres has the form of a symmetric function

$$h(r) = 600 \exp[-0.5(r/r_0)^n], \quad (1)$$

TABLE 1. A summary of the numerical model used in this paper and the representation of physical processes therein, where  $u$  and  $v$  are the horizontal wind components;  $T$  is the absolute temperature and  $T_{ss}$  is the sea surface temperature.

<b>Numerical properties</b>	
Boundary conditions	- <i>Periodic boundary conditions</i> at the eastern and western boundaries - <i>Channel boundary conditions</i> at the northern and southern boundaries - <i>Upper boundary</i> : $\partial u/\partial\sigma = 0$ , $\partial v/\partial\sigma = 0$ , $\partial T/\partial\sigma = 0$ and $\dot{\sigma} = 0$ - <i>Lower boundary</i> : $\dot{\sigma} = 0$ and the $T_{ss} = \text{const.}$ and conditions specified by the boundary-layer formulation
Model grid	- Horizontal: non-staggered Arakawa A-Grid - Vertical: Staggered grid with the horizontal velocity components, geopotential and temperature stored at $\sigma$ -levels and the vertical ‘‘sigma’’ velocity, $\dot{\sigma} = D\sigma/Dt$ , stored half way between $\sigma$ -levels
Vertical resolution	- 30 unequally spaced interior $\sigma$ -levels
Horizontal resolution	- $107 \times 121$ grid points with a grid spacing of 40 km
Top of the domain	- approximately 20 km
Domain size	- <i>Total domain</i> : 4240 km west to east $\times$ 4800 km south to north - <i>Domain of interest</i> : $4000 \times 4000$ km square
Time differencing	- explicit Miller-Pearce (1974) scheme
Spatial differencing	- third-order upwinding advection scheme
Geographic location	- Southern Hemisphere f-plane centred at $20^\circ\text{S}$ latitude
<b>Physical processes</b>	
Radiation processes	- solar radiation (short wave) in to the lower troposphere with diurnal variation (Raymond, 1994) - solar radiation to the surface and terrestrial (long wave) from the surface - atmospheric long-wave radiation to the surface - upward and downward thermal radiation in the troposphere with the Schwarzschild-Schuster approximation (Raymond 1994)
Diabatic processes	- <i>soil</i> : Heat diffusion through three levels in the soil (heat flux into and out of the ground) - <i>surface level</i> : Surface heat budget with prognostic equation for surface temperature - <i>at the lowest atmospheric level</i> : sensible heat flux calculated by similarity theory (stability dependent boundary layer, with eddy diffusivities functions of bulk Richardson number) - <i>above the lowest atmospheric level</i> : Mellor-Yamada 2.25 second-order closure parameterization scheme (1974) (Vertical diffusion above boundary layer based on mixing length hypothesis)
Moisture processes	- no moisture

where  $r$  is the distance in kilometres from the domain centre and  $r_0$  and  $n$  are constants with  $r_0 = 480$  and  $n = 4$ . This function represents a plateau, about 400 km broad, with a maximum height of 600 m (Fig. 1). Calculations are carried out for the case with no surrounding sea, as well as with sea present. Subsequently we refer to these calculations as PNS (plateau/no sea) and PS (plateau/sea), respectively. In further experiments the width of the plateau is varied. The widest plateau ( $r_0 = 640$ ,  $n = 8$ ) has a summit diameter of 800 km (WP) and the Gaussian-like orography (G), with  $r_0 = 400$ ,  $n = 2$  has a simple peak. The model is initialized with the same mean potential temperature profile as in RS, which is based on radiosonde data from Townsville ( $146^\circ\text{E}$ ,  $19^\circ\text{S}$ ). The profile is typical of ocean conditions for the region of interest. As in RS, the constant sea surface temperature  $T_{ss}$  is  $25^\circ\text{C}$  and the surface albedo 0.3. We compare the results of the calculations with orography with those of an experiment with a flat circular land surface surrounded by sea (IS).

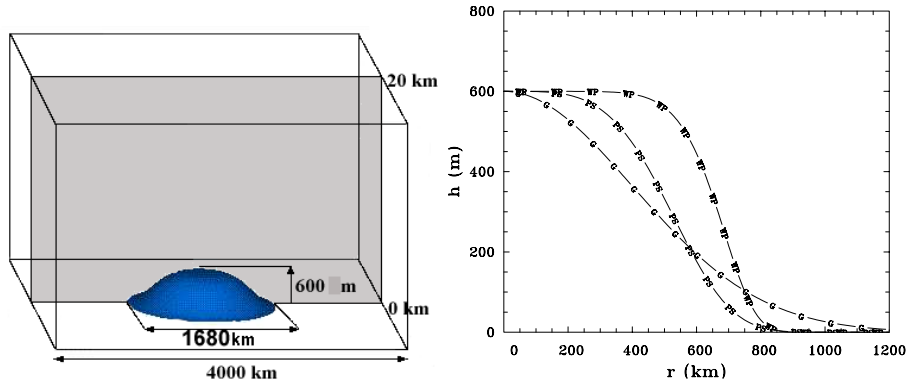


Figure 1. Schematic three-dimensional arrangement of the model with the east-west vertical cross-section through the centre of the plateau (grey area).

TABLE 2. Numerical experiments.

	Shape of the orography	Sea	Diameter of the plateau summit/island
PS	Plateau, given by Eq. (1)	yes	400 km
PNS	Plateau, given by Eq. (1)	no	400 km
IS	Flat circular island	yes	840 km
WP	Wide plateau $h(r) = 600 \exp[-0.5(r/640)^8]$	yes	800 km
G	Gaussian orography $h(r) = 600 \exp[-0.5(r/400)^2]$	yes	0 km

### 3. RESULTS OF THE NUMERICAL EXPERIMENTS

#### (a) Flow evolution

In all calculations the flow is initiated in a quiescent environment by imposed heating. After an initial spin-up period, a mature heat low develops over the land/plateau in all the experiments. During this period the maximum depth of the well-mixed layer over land gradually increases to reach a quasi-steady value, while the actual depth shows a marked diurnal variation. The other variables such as relative vorticity, temperature and wind show also a diurnal variation which becomes repeatable from day to day.

#### (b) Mature stage

We define the mature stage as that stage in which the net heating rate throughout the whole troposphere during a day is nearly zero. In this stage, as during the evolution period, the heat low undergoes a pronounced diurnal cycle. Figure 2 shows the diurnally-averaged vertical profiles of contributions to the net heating rate from solar radiation, terrestrial radiation, horizontal advection and turbulent transfer over the centre of the plateau during a diurnal cycle in the mature stage. The mean vertical distribution of the heating rate due to the terrestrial long-wave radiation is negative. The rate of cooling decreases with height and is effectively zero above 10 km. The magnitude of the cooling in the upper troposphere is significantly underestimated by the grey-atmosphere model. This is due primarily to the neglect of water vapour, which results in strong cooling in these levels. The mean solar radiation tendency is positive in the troposphere and is approximated by a Gaussian profile with a maximum at 4 km (see Eq. A.3 in the Appendix). The heating effect of

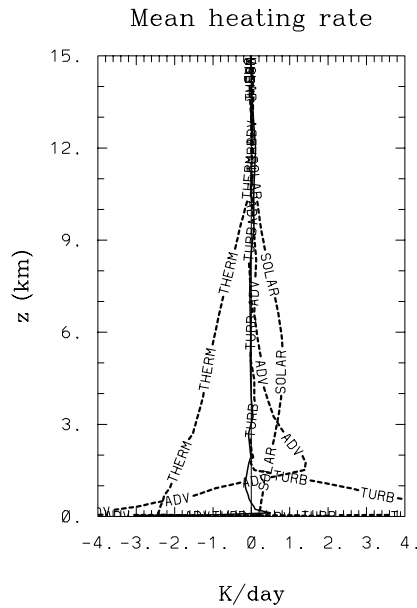


Figure 2. Vertical time-average profiles of potential temperature tendency due to thermal radiation (THERM), solar radiation (SOLAR), advection (ADV), and convective turbulence (TURB). The residual heating is shown by an unmarked line, which is barely visible above 1.5 km because it lies very close to the axis.

ozone in the stratosphere is ignored. The long- and short-wave radiative heating tendencies are similar to those shown by Raymond (1994) and are realistic in the lower troposphere. Turbulent transfer is important in the first kilometre, whereas the advective contribution extends up to a height of 5 km. The sum of the tendencies is indicated by the solid line and is approximately zero; there is almost no residual heating. Starting with the mature state conditions at 6 am, the model is integrated for a two-day period so that continuous segments of a diurnal cycle may be illustrated.

The first calculations are carried out for the case with orography in the middle of the domain with no surrounding sea (designated PNS) as well as with sea present (designated PS). The shape of the orography is defined by Eq. 1. We show the results of the two experiments side by side in order to highlight the role of the sea and the orography. In some cases we show also the results for the circular heated flat island (designated IS).

(c) *Sea/land breeze*

Figure 3 shows time-height series of zonal wind up to a height of 4 km at a point just inland from the coast for a one day sequence. The heating of the lower troposphere through dry convection over land leads to a horizontal density difference that in turn results in a flow circulation akin to a sea breeze, with air flowing from the ocean towards the warmer land. The left panel in figure 3 shows the fully developed sea breeze circulation at the coast in the case of the circular island (Expt. IS). The sea breeze begins about 1400 h and has a maximum strength in the evening at about 2100 h, but its maximum depth of about 1.2 km occurs in the late afternoon. The associated return flow aloft is a prominent feature between 1 and 3 km. The sea breeze is replaced by a land breeze at about 0400 h, which persists until the sea breeze onset on the following day. In this case the land breeze is

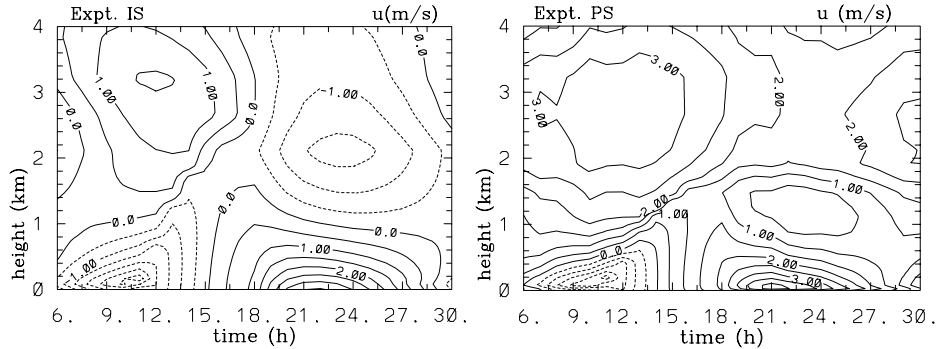


Figure 3. Time-height cross-sections of the zonal wind up to a height of 4 km just inland from the coast for Expt. IS in the left panel and Expt. PS in the right panel for a one day sequence from 0600 h. Contour intervals are  $0.5 \text{ ms}^{-1}$ . Solid (dashed) contours indicate positive (negative) or landward (seaward) values.

rather weaker than the sea breeze. In the case PS the sea breeze starts a little later than in Expt. IS, at about 1400 h, and remains until about 0600 h (Fig. 3, right), when it is again replaced by a land breeze circulation. The maximum wind speed in the sea breeze regime is a little stronger than in Expt. IS and the maximum wind speed is located higher. The land breeze is comparable in strength with the sea breeze, but its depth is shallower than in the case IS, reaching to a maximum height of 600 m. What is seen as the upper return circulation of the sea breeze in the left panel in Fig. 3 appears now as a region of reduced onshore flow; it is dominated by the broader scale circulation induced by the topography. Note that in the mature stage, the individual flow components such as the sea breezes are not growing in a quiescent environment, but rather in a broader scale flow to which they and other components contribute; henceforth we refer to this broadscale flow as *the broadscale circulation associated with the heat low*.

(d) *Wind on the slopes*

The flow in the presence of orography is more complicated than it is over a flat island as anabatic winds develop over the slopes during the day and shallow katabatic winds during the night, both affecting the flow over the plateau and the broadscale circulation associated with the heat low. The left panel of Fig. 4 shows time-height isotachs of zonal wind up to a height of 4 km at a point midway up the slope (about 300 km inland) for a one day sequence for the case PS and the right panel shows the corresponding isotachs for the case of a plateau without sea (PNS). During the day, absorption of solar radiation warms the air near the land surface and the air near the sloping ground becomes warmer than that in the free atmosphere at the same height. The warmer air flows from the lowland up the slope as an anabatic wind. The onshore flow seen in Fig. 4a is a combination of the anabatic wind, the sea breeze and the broadscale vertical circulation due to the established heat low. It is stronger and deeper than the sea breeze at the coast and reaches a maximum strength at 2330 h, two and a half hours later than the sea breeze in Fig. 3a. The subsiding, offshore flow (dashed contours) over the slope starts at about 0500 h and persists until about 1400 h; it is essentially a land breeze and is associated with subsidence over the plateau. The subsidence over the slope at night in Expt. PNS (Fig. 4b) is absent on account of the absence of sea. The anabatic wind during the daytime is stronger than in Expt. PS because with no sea there is no land breeze to weaken the flow. In both these calculations there is no evidence of a shallow katabatic wind and we conclude that such a wind is either too shallow to be resolved by the model or, more likely, that it is dominated by the broadscale circulation associated with the heat low.

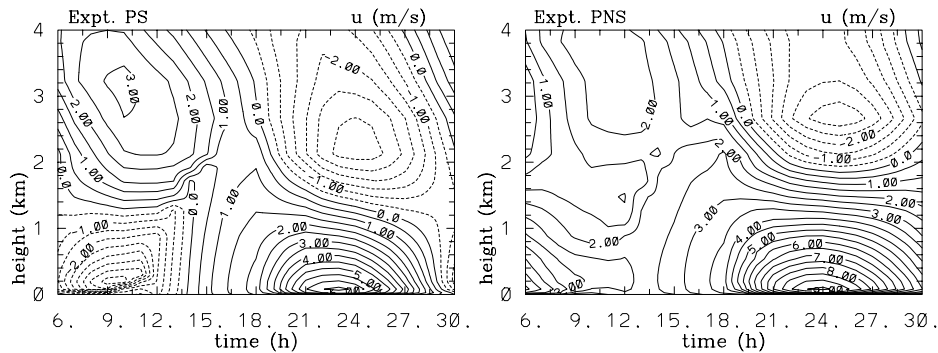


Figure 4. Time-height cross-sections of the zonal wind up to a height of 4 km on the slope in Expt. PS in the left panel and in Expt. PNS in the right panel for a one day sequence from 0600 h. Contour intervals are  $0.5 \text{ ms}^{-1}$ . Solid (dashed) contours indicate positive (negative) or slope upward (slope downward) values.

We consider now the spatial structure of the flow in a vertical west-east cross-section through the centre of the plateau (indicated by the grey rectangle in Fig. 1) at selected times of day during the mature stage of the heat low. Figures 5 - 12 show a series of such cross-sections at 1500 h, 0000 h, 0300 h and 0800 h. As in Fig. 4 we adopt the convention that the left panels show the case with surrounding sea and right panels without sea. The main features of a diurnal cycle in the two experiments are as follows.

(e) *Afternoon conditions*

During the day a convectively well-mixed layer builds up over the land in each case. In Expt. PS, the isolines of zonal wind show a complex structure at 1500 h (Fig. 5, left). The beginnings of the sea breeze are evident at very low levels near the coast beneath the remnants of the land breeze circulation. There is a well-developed anabatic flow over the slopes of the orography. The last remnants of the outflow associated with subsidence over the plateau are still in evidence above the plateau, itself. In Expt. PNS (Fig. 5, right), the sea breeze is absent and no land breeze occurs that could weaken the anabatic circulation. Thus the maximum onshore wind is larger than in Expt. PS.

The isotachs of the meridional wind speed are shown in Fig. 6. The solid contours at low levels indicate a southerly flow (i.e. motion into the page), while the dashed contours show northerly flow. Thus a cyclonic circulation appropriate to the Southern Hemisphere occurs over the slopes and the plateau in both experiments, with the maximum speed occurring near the top of the slope. At larger heights, the meridional wind becomes anticyclonic. In Expt. PS the maximum occurs above the coastline at a height of 2.5 km, while in Expt. PNS it occurs higher and further inland and the maximum speed is larger.

(f) *Nighttime conditions*

At night the air over the land stabilizes at low levels on account of the continued inland penetration of sea breeze air, the radiative cooling of the free atmosphere and the turbulent transport of heat to the radiatively-cooled ground. The stabilization of the air near the ground leads to the formation of the pronounced nocturnal low-level jet over land (note that the steepness of the terrain is greatly exaggerated in all the figures: in reality the rise of 600 m occurs over a horizontal distance of about 350 km).

Figures 7 and 8 show the isotachs of zonal wind and vertical wind speed, respectively,

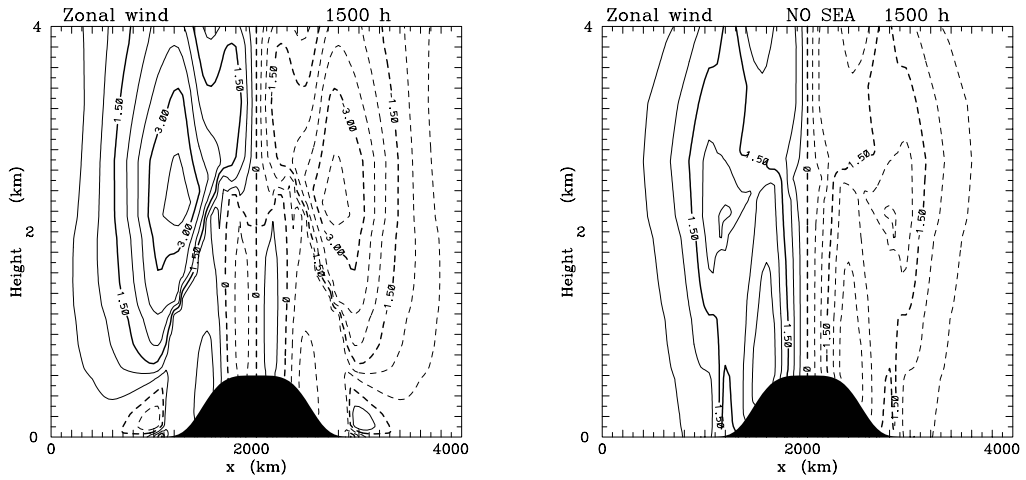


Figure 5. Vertical west-east cross-sections of the zonal wind (contour interval  $0.5 \text{ ms}^{-1}$ ) up to a height of 4 km at 1500 h in the mature stage of the calculation with sea (PS) in the left panel, and with no sea (PNS) in the right panel.

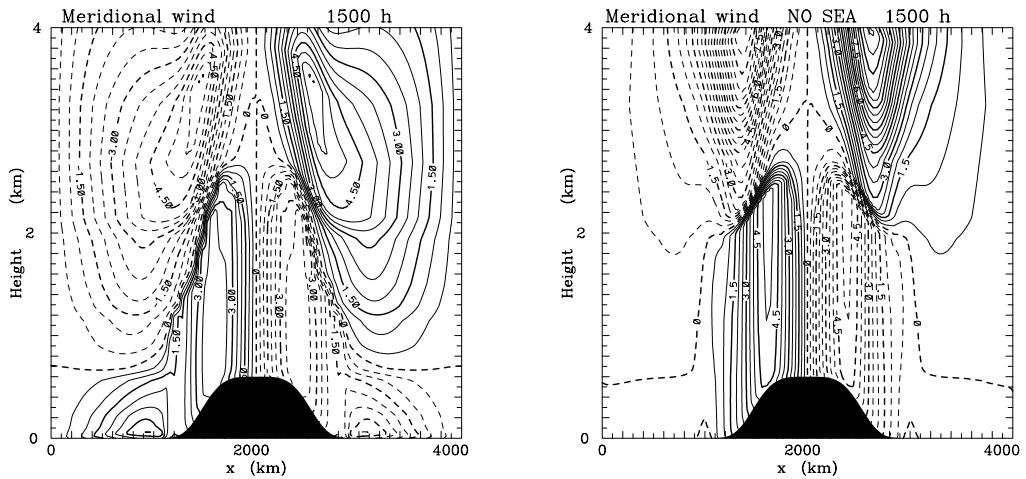


Figure 6. Vertical west-east cross-sections of the meridional wind (contour interval  $0.5 \text{ ms}^{-1}$ ) up to a height of 4 km at 1500 h in the mature stage of the calculation with sea (PS) in the left panel, and with no sea (PNS) in the right panel.

for Expts. PS and PNS at 0000 h. At this time there is a strong inland flow above the slope with the maximum on the upper half of the slope. This flow is stronger and deeper in Expt. PNS, and the maximum occurs near the top of the slope in this case. There is an offshore return flow aloft extending to a height of about 4 km in Expt. PS and to a height of about 5 km in Expt. PNS (not indicated in the figure).

Strong ascent occurs in two broad "plumes" near the edges of the plateau, these regions have the form of a symmetrical elliptical annulus in the three-dimensions. The subsidence over the slopes, indicated by dashed lines, is strongest in Expt. PNS.

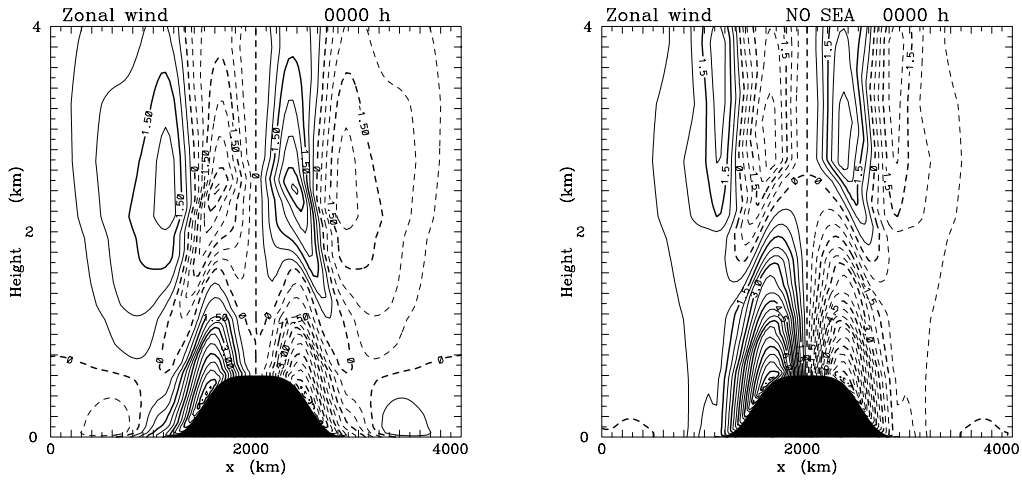


Figure 7. Vertical west-east cross-sections of the zonal wind (contour interval  $0.5 \text{ ms}^{-1}$ ) up to a height of 4 km at 0000 h in the mature stage of the calculation with sea (PS) in the left panel, and with no sea (PNS) in the right panel.

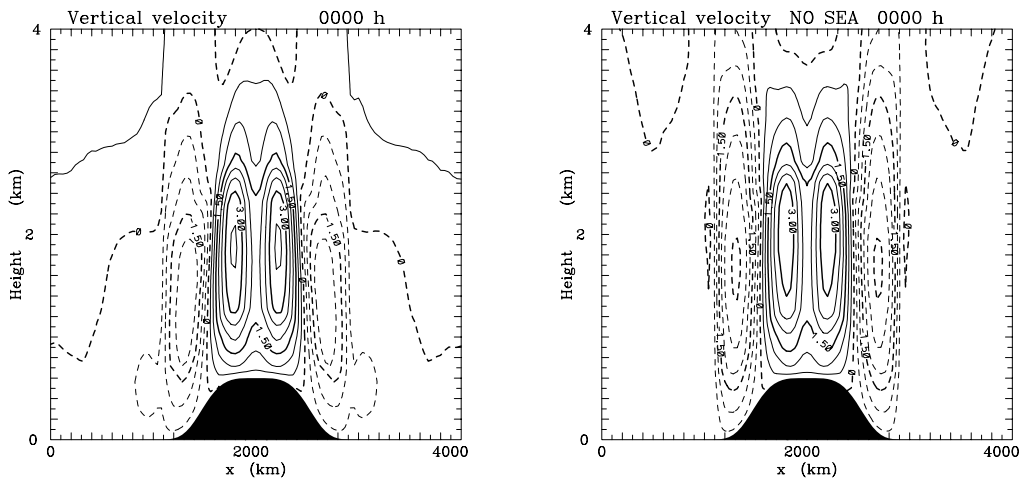


Figure 8. Vertical west-east cross-sections of the vertical velocity (contour interval  $0.5 \text{ cms}^{-1}$ ) up to a height of 4 km at 0000 h in the mature stage of the calculation with sea (PS) in the left panel, and with no sea (PNS) in the right panel.

(g) *Early morning conditions*

The early morning hours are characterized by a rapid increase in the low-level relative vorticity in the early morning hours as shown in Fig. 9. The relative vorticity signature above the plateau is weak during the afternoon when the convective mixing is at its peak, but its magnitude increases steadily after sunset (figure not shown). This behaviour is similar to that in the case without orography discussed by RS. At 0300 h the vorticity is strong and cyclonic over the plateau in both cases as indicated by the dashed contours in Fig. 9. In Expt. PS the vorticity is cyclonic below 2.5 km and anticyclonic above this level (Fig. 9, left panel), while in Expt. PNS it remains cyclonic to a height of 3 km (Fig. 9, right panel). The relative vorticity signature has a maximum at 0400 h in Expt. PNS and about 0500 h in Expt. PS in both cases at a height of about 100 m, indicating a strong

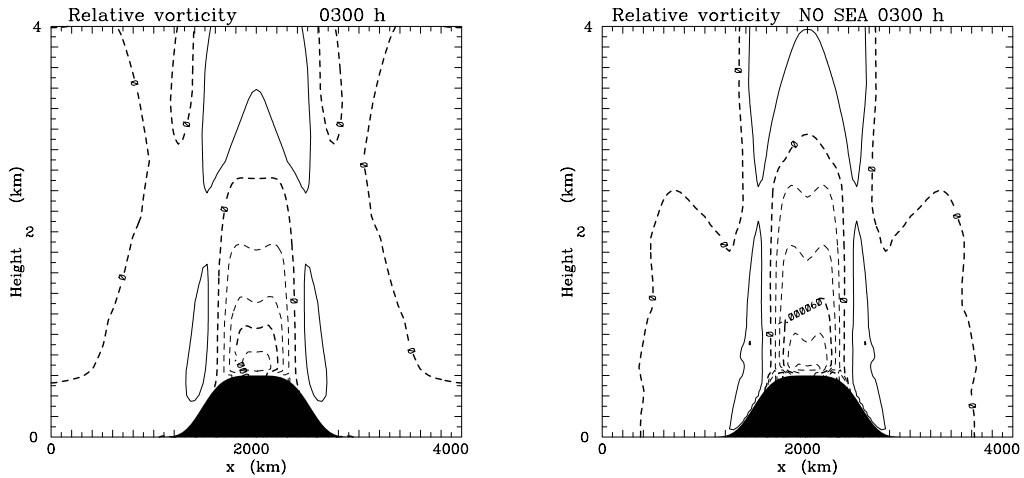


Figure 9. Vertical west-east cross-sections of the relative vorticity (contour interval  $2 \times 10^{-5} \text{s}^{-1}$ ) up to a height of 4 km at 0300 h in the mature stage of the calculation with sea (PS) in the left panel, and no sea (PNS) in the right panel.

connection with the nocturnal low-level jet.

A prominent feature of the potential temperature field is the development of a deep well-mixed layer during the afternoon. The remnants of this layer, characterized by uniform potential temperature, are still evident at night over the top of the plateau and also over the surrounding plain in the case without sea. The isolines in both panels of Fig. 10 show the residue of the well mixed layer at 0300 h, which attains a depth of about 3.5 km in Expt. PS (Fig. 10, left panel) and more than 4 km in Expt. PNS (Fig. 10, right panel). During the night a low-level stable layer develops, gradually deepening to about 200 m around sunrise. Stabilization of the near-surface layers recommences at night because of the horizontal advection of cooler air on to the plateau and the mechanically-forced turbulent heat flux to the cooler ground surface. The simple radiation scheme used here was added to the present version of the model to prevent an upward drift in mean temperature during many days of model integration, but it is not capable of producing a large radiative-flux divergence near the surface (see the profile of cooling shown in Fig. 2). Thus we do not see the development of a shallow nocturnal inversion over the plain in Expt. PNS as near-surface wind speeds are small there. The inversion and mixed-layer depths over the plateau are nevertheless characteristic of those observed over central Australia, for example, during the late dry season (Smith *et al.*, 1995).

(h) *After sunrise*

In Expt. PS a land breeze develops around sunrise (right panel of Figs. 3, left panel of 4). The isotachs of zonal wind speed in this experiment at 0800 h show the downslope motion over a depth of about 2 km with a maximum over the rim of the plateau (Fig. 11, left panel). At very low levels a shallow anabatic flow is evident. In the case without sea the land breeze is absent (Fig.11, right panel).

The contour lines in Fig. 12 show the vertical component of flow as in Fig. 8. Subsidence over the plateau is strongest in Expt. PNS, as indicated by the narrow strip of dark shading above the centre of the plateau, but it occurs also in Expt. PS. This subsidence feeds the low-level downslope flow above the plateau in Expt. PS. Adjacent to the subsidence region



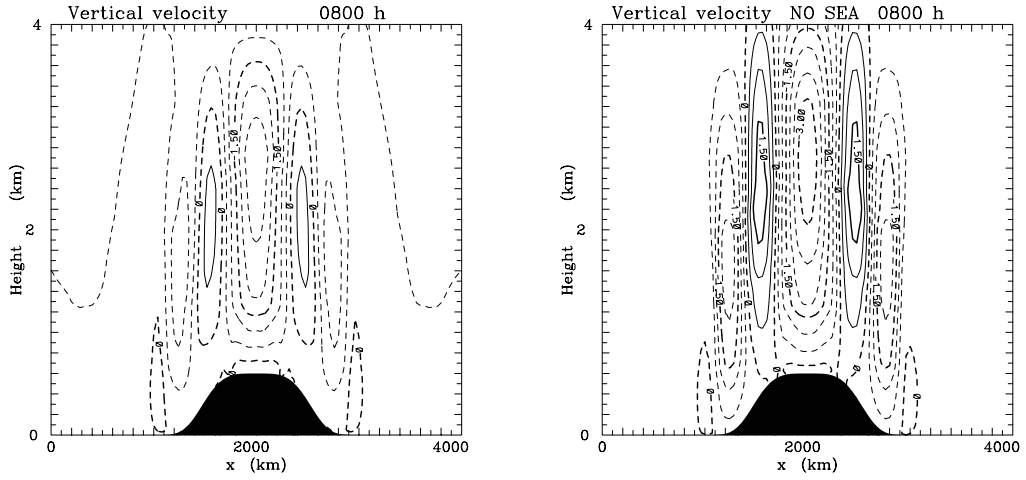


Figure 12. Vertical west-east cross-sections of vertical wind (contour interval  $0.5 \text{ cms}^{-1}$ ) up to a height of 4 km at 0800 h in the mature stage of the calculation with sea (PS) in the left panel, and no sea (PNS) in the right panel.

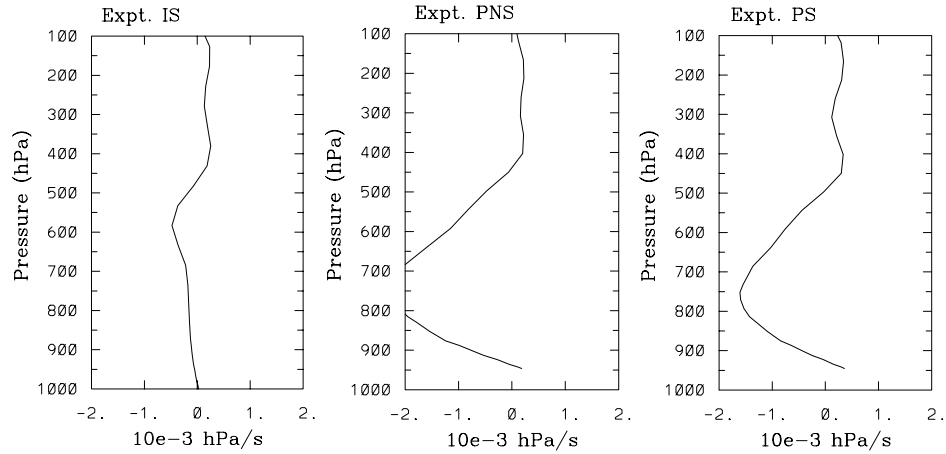


Figure 13. Vertical pressure velocity ( $\omega(p)$ ) as a function of pressure at 2000 h at a location 160 km from the domain centre: left panel, case IS; middle panel, case PNS; and right panel, case PS.

profiles, which are based on data collected during the Monsoon Experiment (MONEX) in 1979, show ascending motion only below the 800 hPa level, even during the day. Subsidence at upper levels is a persistent feature of these observations. The terrain in the region where the most of measurements were made is relatively flat with variations on the order of two hundred meters over six hundred kilometres.

Figure 13 shows profiles of  $\omega(p)$  for Expts. IS, PNS and PS at a location 160 km from the domain centre. Over the flat island the vertical motion is relatively weak, while in the cases with orography, ascent occurs over a deep layer, up to 500 hPa, as in the observations reported by Hart (1990). These differences show that that orography plays an important role determining the pattern of vertical motion above the heat low and suggest that the differences in vertical motion diagnosed by Blake *et al.* (1983) and Hart *op. cit.* could be a result of the differences in orography in the two regions of study.

*(j) Variation of the width of the plateau*

Further experiments, in which the width of the plateau is varied show that the nocturnal low-level jet is a prominent feature in all cases. We summarize the salient results of these without showing figures. Over the wider plateau (Expt. WP) a shallower mixed layer develops during the day. At nighttime the upward motion and relative vorticity signatures are weaker than in Expt. PS. The nocturnal low-level jet develops more strongly, but does not reach the middle of the plateau. The well-mixed layer is deepest in the calculation with Gaussian-orography (Expt. G) and at night the inversion layer is well developed over the entire land mass. Moreover, the upward motion in the evening is stronger than in the other calculations with orography, and is accompanied by a stronger cyclonic relative vorticity signature at that time.

## 4. CONCLUSIONS

We have investigated the dynamics of a heat low in the presence of orography using an idealized numerical model with a boundary-layer parameterization and a simplified representation of radiative transfer. The calculations reproduce the main observed properties of heat lows occur over elevated terrain including: the lowest minimum pressure in the late afternoon; a cyclonic circulation at low levels; a divergent anticyclonic circulation aloft.

In all the calculations a convectively well-mixed layer builds up over the land and has a maximum depth in the case of the plateau not surrounded by sea. The maximum zonal velocity in a vertical cross-section through the domain centre is the highest in this case and it is the weakest in the calculation over a flat island. In the latter case the zonal velocity shows regions of strong onshore flow near the two coastlines marking the coastal sea breezes. In the calculations with a plateau the sea breezes are weaker and there is an anabatic wind over the orographic slopes.

The presence of a nocturnal low-level jet over land is a prominent feature in all calculations. The low-level wind maximum over the flat island is weaker than that over the plateau and the relative vorticity signature is strongest at night in the case with a plateau surrounded by sea because the remnants of the anabatic wind reinforce the low-level convergence.

The pattern of vertical motion has a richer structure in the cases with orography, and this structure does not have a significant diurnal variation. The vertical motion over the plateau is strongest in the case with no sea; in the other cases it is inhibited by the stronger static stability that occurs over the sea. The presence of orography leads to a deeper mixed layer and higher wind speeds. The top of the well-mixed layer is higher over the plateau than over the plain. These differences provide an explanation for such different vertical structures that have been observed above heat lows over Saudi Arabia and over northwestern Australia.

The width of the plateau influences the wind strength over the plateau and the magnitude of the relative vorticity. Over a relatively narrow plateau, for example, in the case with Gaussian-orography, ascending motion is stronger at night than over a wider plateau because the slope winds reinforce the upward flow above the terrain peak. The vorticity signature is stronger in this case also. In contrast, the nocturnal jet is strongest when the flow is able to spread out horizontally above the plateau.

## REFERENCES

- Adams, M. 1993 A linear study of the effects of heating and orography on easterly airstreams with particular reference to northern Australia. *Aust. Met. Mag.*, **42**, 69-80
- Blake, D. W., T. N. Krishnamurti, S. V. Low-Nam and J. S. Fein 1983 Heat low over the Saudi Arabian desert during May 1979 (Summer MONEX). *Mon. Wea. Rev.*, **111**, 1759-1775
- Charney, J. G. 1975 Dynamics of deserts and drought in the Sahel. *Q. J. R. Meteorol. Soc.*, **101** 193-202
- Fandry, C. B. and L. M. Leslie 1984 A two-layer quasi-geostrophic model of summer trough formation in the Australian subtropical easterlies. *J. Atmos. Sci.*, **41**, 807-181
- Gaertner, M. A., C. Fernández and M. Castro 1993 A two-dimensional simulation of the Iberian summer thermal low. *Mon. Wea. Rev.*, **121**, 2740-2756
- Hart, T. L. 1990 Estimates of horizontal divergence and vertical velocity over northern Australia, and implications for biogeophysical feedback. *Aust. Met. Mag.*, **38**, 107-122
- Manabe, S. and R. F. Strickler 1964 Thermal equilibrium of the atmosphere with a convective adjustment. *J. Atmos. Sci.*, **21**, 361-385
- Mellor, G. and T. Yamada 1974 Hierarchy of a turbulent closure models for planetary boundary layers. *J. Atmos. Sci.*, **31**, 1791-1806
- Miller, M. J. and R. P. Pearce 1974 A three-dimensional primitive equation model of cumulonimbus convection. *Q. J. R. Meteorol. Soc.*, **100**, 133-154
- Otterman, J. 1974 Baring high-albedo soils by overgrazing: a hypothesized desertification method. *Science*, **186**, 531-3
- Raymond 1994 Convective processes and tropical atmospheric circulations. *Q. J. R. Meteorol. Soc.*, **120**, 1431-1455
- RÁCZ Zs. and R. K. Smith 1999 The dynamics of heat lows. *Q. J. R. Meteorol. Soc.*, **125**, 225-252
- Smith, R. K., M. J. Reeder, N. J. Tapper and D. R. Christie 1995 Central Australian cold fronts. *Mon. Wea. Rev.*, **123**, 16-38

## APPENDIX

## (a) Radiation scheme

The simple parameterization scheme for radiation is that designed by Raymond (1994) for idealized studies of tropical weather systems. The thermodynamic equation in  $\sigma$ -coordinates has the form

$$\frac{DT}{Dt} = \frac{RT}{c_p} \left( \frac{D \ln p_s}{Dt} + \frac{\dot{\sigma}}{\sigma} \right) + (\dot{Q}_{heat} + \dot{Q}_{diff}) \left( \frac{\sigma p_s}{p_o} \right)^{\frac{R}{c_p}}, \quad (\text{A.1})$$

where  $R$  is the specific gas constant,  $T$  the absolute temperature,  $c_p$  the specific heat capacity at constant pressure,  $p_s$  the surface pressure,  $\dot{\sigma} = D\sigma/Dt$  the vertical “ $\sigma$ -velocity”,  $p_o = 1000$  hPa the reference pressure, and  $\dot{Q}_{heat}$  represents the contributions to the total heating from radiative processes and from the flux of sensible heat and  $\dot{Q}_{diff}$  represents the horizontal diffusion of heat. Eq. A.2) gives the contribution of the flux of sensible heat  $F_H$  to the atmosphere and the second term  $r$  is the temperature tendency due to radiation.

$$\dot{Q}_{heat} = -\frac{1}{\rho c_p} \frac{\partial F_H}{\partial z} + \underbrace{\frac{\theta}{\rho c_p T}}_r (Q_{therm} + Q_{sol}), \quad (\text{A.2})$$

where  $\rho$  is the density,  $z$  the vertical distance,  $\theta$  the potential temperature. The term  $r$  is divided into two parts, thermal and solar radiation. The grey-atmosphere model is used for long-wave radiation, while a fixed heating profile is taken for the short-wave component.

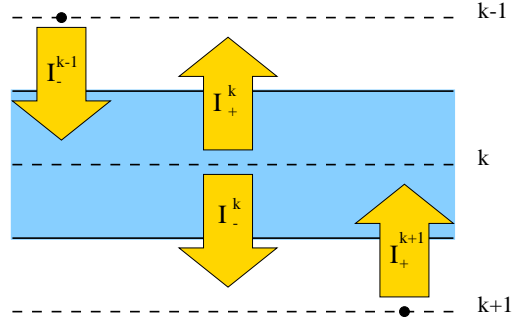


Figure A.1. Schematic diagram showing the radiative transfers between a particular model layer (characterized by level number  $k$  and the two adjacent layers designated by  $k - 1$  and  $k + 1$ . The arrows represent the radiative heat flux to and from the level  $k$ .

The solar component of radiation causes significant heating in the lower atmosphere. Following Manabe and Strickler (1964) it can be approximated by the Gaussian profile:

$$Q_{sol} = \cos(\lambda_0) Q_{max} \exp \left[ -\frac{(z - z_{max})^2}{z_w^2} \right], \quad (\text{A.3})$$

where  $Q_{max}$  is a fixed maximum enthalpy per unit volume and time,  $\lambda_0$  is the solar zenith angle,  $z_{max}$  is the fixed height of the maximum heating and  $z_w$  a fixed height. The diurnal variation is given by  $\cos(\lambda_0)$ . The heating effect of ozone in the stratosphere is ignored.

The thermal radiation is represented by a grey-body scheme:

$$Q_{therm} = \frac{d}{dz} (I_+ - I_-) = \frac{dI_+}{dz} - \frac{dI_-}{dz} = \mu \rho (2\sigma_{sb} T^4 - I_+ - I_-) \quad (\text{A.4})$$

$$\frac{dI_+}{dz} = \rho \mu (\sigma_{sb} T^4 - I_+) \quad \frac{dI_-}{dz} = -\rho \mu (\sigma_{sb} T^4 - I_-) \quad (\text{A.5})$$

The upward and downward radiative fluxes ( $dI_+/dz$  and  $dI_-/dz$ ) can be obtained by the Schwarzschild-Schuster approximation (Eq. A.5), where  $\mu$  is the clear-air infrared absorption coefficient and  $\sigma_{sb}$  the Stefan-Boltzmann constant. Fig. A.1 shows that each layer radiates heat downwards and upwards and receives heat radiation from neighbouring layers.

(b) *Parameters*

Parameter	Value	Comment
$R$	$287.04 \text{ m}^2 \text{ s}^{-2} \text{ K}^{-1}$	Specific gas constant for dry air
$c_p$	$1004.67 \text{ m}^2 \text{ s}^{-2} \text{ K}^{-1}$	Specific heat of dry air at constant pressure
$p_0$	1000 hPa	Reference pressure
$z_{max}$	4000 m	Fixed height of the maximal heating
$z_w$	4000 m	Fixed height
$\mu$	$3 \cdot 10^{-4} \text{ m}^2 \text{ kg}^{-1}$	Clear-air infrared absorption coefficient
$\sigma_{sb}$	$5.67 \cdot 10^{-8} \text{ W m}^{-2} \text{ K}^{-4}$	Stefan-Boltzmann constant